DE GRUYTER Science and Engineering of Composite Materials 2021; 28: 628–637

Research Article

Yu-qiang Cheng, Chang-geng Shuai* and Hua Gao

Research on the mechanical model of cord-reinforced air spring with winding formation

https://doi.org/10.1515/secm-2021-0060
received July 24, 2021; accepted October 03, 2021

Abstract: In this article, the parametric model for the stiffness characteristic and burst pressure of cord-reinforced air spring with winding formation is developed. Based on the non-geostrophic winding model and the assumption of cord cross-stability, the cord winding trajectory model of the capsule is established. Then, the anisotropic and nonlinear mechanics model of the capsule with complex cord winding trajectory variation characteristics is constructed by the classical thin-shell theory. The capsule state vector is solved by the extended homogeneous capacity precision integration method. Due to the complex coupling relationship between the capsule state vector and the internal air pressure, the stiffness characteristic is solved by the iterative integration method. The burst pressure of the air spring is solved by the Tsai–Hill strength theory. Eventually, the accuracy and reliability of the proposed method are verified by the experimental results. The effects of the material properties, winding parameters, and geometric structure parameters on stiffness characteristics and burst pressure are discussed. The results of this article provide an important theoretical basis for the performance design of cord-reinforced air springs with winding formation.

Keywords: air spring, cord winding, theory of thin shell, transfer matrix method, stiffness, burst pressure

* **Corresponding author: Chang-geng Shuai,** Institute of Noise & Vibration, Department of Power Engineering, Naval University of Engineering, Wuhan 430033, China; State Key Lab of Ship Vibration & Noise, Wuhan 430033, China, e-mail: chgshuai@163.com
Yu-qiang Cheng, Hua Gao: Institute of Noise & Vibration, Department of Power Engineering, Naval University of Engineering, Wuhan 430033, China; State Key Lab of Ship Vibration & Noise, Wuhan 430033, China

1 Introduction

The air spring uses the nonlinear stiffness and damping characteristics of air compression to isolate vibration and shock. It has been widely used in the field of vibration and noise reduction in vehicles and ships [1–3]. The capsule of the air spring generally consists of a cord skeleton layer and a rubber layer. The cord skeleton layer is the main force carrier of the capsule, and it is formed by high-strength cords and rubber [4,5]. In applications with small installation space and large bearing requirements, the air spring must achieve a large bearing capacity at a small size. Therefore, its internal pressure is generally 4–6 times higher than general air springs. The cord-reinforced air spring with winding formation is proposed to ensure the structural strength of the air spring under high pressure.

The mechanical characteristics of air springs consist mainly of stiffness characteristics and burst pressure. The effects of geometric parameters, internal pressure, and material parameters on the mechanical characteristics of air springs are difficult to ignore [6–8]. The capsule of an air spring composed of rubber-cord composites is typical anisotropic materials with complicated mechanical modeling. Therefore, most scholars established the mechanical model of the capsule by simplification, analogy, or simulation. Erin et al. simulated the nonlinearity of the capsule with a linear spring, a damper, and a hysteresis damper in parallel to analyze the mechanical properties of the air spring [9]. Moon and Lee et al. extracted the mechanical property data of rubber air springs. The Zener model was used to simulate the mechanical properties of air springs. However, the model is complicated and less general [10]. Wong et al. developed a finite element model of the air spring. The nonlinear properties of the capsule were described by ABAQUS and rebar elements. The effects of the cord winding angle, cord diameter, and the initial internal pressure on the mechanical properties were analyzed [11].

Due to the characteristics of the forming process of the air spring, the air spring capsule not only has complex anisotropic and nonlinear characteristics but also presents complex winding trajectory variation characteristics. It makes the construction of a mechanical model of the air spring extremely difficult. The cord trajectory inside the air spring capsule is determined by two stages: the cord winding stage and the capsule extrusion stage. Currently, most scholars have conducted in-depth theoretical studies on the cord winding stage. Based on the geodesic and nongeodesic winding models, the cord winding models of different curvature shells and the corresponding winding process methods were analyzed [12–15]. However, there is a lack of relevant theoretical studies on the changes in cord winding trajectory during the capsule extrusion stage. In addition, there is a strong coupling between the capsule state vector and the internal pressure of the air spring in the process of solving the mechanical properties of the air spring. The capsule state vector (internal force and displacement, etc.) changes with the internal pressure, and the internal pressure is also affected by the change in the capsule state vector. The complexity of solving the mechanical properties of air springs is further increased. Therefore, establishing the mechanical model of the rubber-cord composite capsule with complex winding trajectory variation characteristics and solving the mechanical characteristics of the air spring under strong coupling of the capsule state vector and the internal pressure are difficult points in the study of the parametric mechanical model of the cord-reinforced air springs with winding formation.

The main purpose of this article is to develop the parametric model for the stiffness characteristics and burst pressure of the cord-reinforced air spring with winding formation. Some new methods for constructing and solving mechanics models of the cord-reinforced air spring are presented. Some crucial parameter studies of the cord-reinforced air spring are also reported. These results provide an important theoretical basis for the performance design of the cord-reinforced air spring with winding formation.

2 Theoretical model

2.1 Geometry model of the air spring

The air spring mainly consists of the top plate, capsule, base plate, and constraint sleeve, as shown in Figure 1. In the figure, P is the internal pressure, F is the bearing capacity of the air spring, α and β are the upper and lower guiding angles of the air spring capsule, respectively, R_e is the effective radius of the air spring, and *abcd* is a microelement on the capsule. The air spring capsule is simplified to a rotational shell formed by a plane curve rotating around an axis coplanar with the curve, and the curve is the meridian. The coordinates of any point on the shell can be expressed by (φ, θ), φ represents the direction of meridian, and θ represents the direction of latitude. The corresponding principal radius of curvature is expressed by R_φ and R_θ, respectively, and the lame coefficients of the rotational shell are R_0 and R_φ. The following parametric equations can be obtained from the geometric structure relations:

$$\begin{cases} R_\theta = R_\varphi + \dfrac{R_e}{\sin\varphi}, & \alpha \le \varphi \le \pi \\ R_\theta = -R_\varphi - \dfrac{R_e}{\sin\varphi}, & \pi < \varphi \le 2\pi - \beta \\ R_0 = R_\theta \sin\theta. \end{cases} \tag{2.1}$$

2.2 Material model of the air spring

The air spring capsule is the rubber-cord composite. It is formed by alternating layers of rubber and cord. However, since the elastic modulus of the cord in the capsule is much larger than that of the rubber, the effect of the elastic modulus of the rubber will be ignored in the subsequent analysis. Let N_φ, N_θ, and $N_{\varphi\theta}$ represent the film internal force components, and M_φ, M_θ, and $M_{\varphi\theta}$ represent

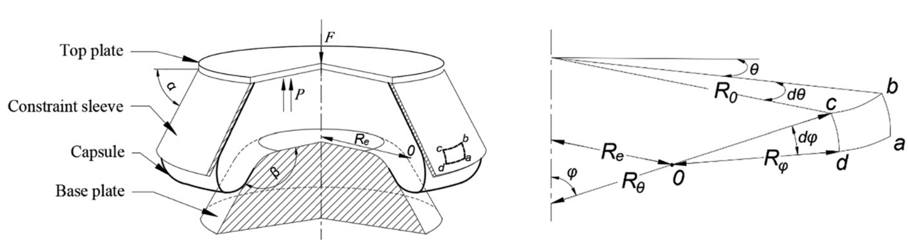

Figure 1: Schematic diagram of the air spring structure.

the bending internal force components. According to the theory of composite laminated plate theory [16], the relationship between the internal force in the capsule and the midsurface strain can be expressed as

$$\begin{Bmatrix} N_\varphi \\ N_\theta \\ N_{\varphi\theta} \end{Bmatrix} = \begin{bmatrix} A_{11} & A_{12} & \\ A_{12} & A_{22} & \\ & & A_{66} \end{bmatrix} \begin{Bmatrix} \varepsilon_\varphi \\ \varepsilon_\theta \\ \gamma_{\varphi\theta} \end{Bmatrix}, \tag{2.2}$$

$$\begin{Bmatrix} M_\varphi \\ M_\theta \\ M_{\varphi\theta} \end{Bmatrix} = \begin{bmatrix} D_{11} & D_{12} & \\ D_{12} & D_{22} & \\ & & D_{66} \end{bmatrix} \begin{Bmatrix} \chi_\varphi \\ \chi_\theta \\ \chi_{\varphi\theta} \end{Bmatrix}. \tag{2.3}$$

In equations (2.2) and (2.3), A_{ij} is the tensile stiffness and D_{ij} is the bending stiffness. The equation of stiffness can be expressed as

$$\begin{cases} A_{ij} = \bar{Q}_{ij} h \\ D_{ij} = \bar{Q}_{ij} \dfrac{h^3}{12} \end{cases} \tag{2.4}$$

In equation (2.4), h is the total thickness of the cord and $\bar{Q}_{ij}$ is the stiffness coefficient of the capsule in the nonmaterial principal direction, and can be expressed as

$$\begin{cases} \bar{Q}_{11} = Q_{11}\cos^4\delta + 2(Q_{12} + 2Q_{66})\sin^2\delta\cos^2\delta \\ \qquad + Q_{22}\sin^4\delta, \\ \bar{Q}_{12} = (Q_{11} + Q_{22} - 4Q_{66})\sin^2\delta\cos^2\delta + Q_{12}(\sin^4\delta \\ \qquad + \cos^4\delta), \\ \bar{Q}_{22} = Q_{11}\sin^4\delta + 2(Q_{12} + 2Q_{66})\sin^2\delta\cos^2\delta \\ \qquad + Q_{22}\cos^4\delta, \\ \bar{Q}_{66} = (Q_{11} + Q_{12} - 2Q_{12} - 2Q_{66})\sin^2\delta\cos^2\delta \\ \qquad + Q_{66}(\sin^4\delta + \cos^4\delta), \end{cases} \tag{2.5}$$

In equation (2.5), E_1 and E_2 are the elastic modulus of the cord in the 1, 2 directions, respectively, v_{12} and v_{21} are Poisson's ratio of the cord in the 1-2 and 2-1 directions, respectively, G_{12} is the shear modulus of the cord, and δ is the winding angle of the cord in the capsule.

2.3 Winding model of the air spring

As shown in Figure 2, the forming core mold of the air spring can be simplified to the combination of the front-end revolving body and the back-end revolving body. The front-end revolving body forms the circular section of the air spring capsule in Figure 1, and the back-end revolving body forms the straight section of the air spring capsule in Figure 1.

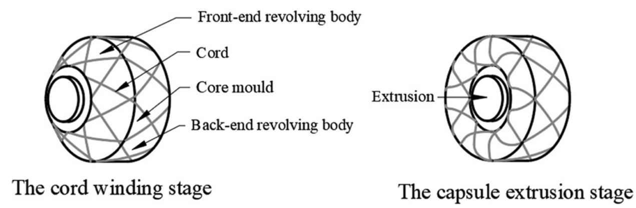

Figure 2: The main forming process of the air spring.

2.3.1 Cord trajectory model in the cord winding stage

Since the air spring linear section capsule is in direct contact with the constraint sleeve of the air spring, the subsequent mechanical analysis only considers the mechanical action of the circular section capsule. Therefore, the model of the cord winding trajectory on the front-end revolving body of the core mold needs to be established. The front-end revolving body can be regarded as a conical shell structure, and its geometric model is shown in Figure 3. Taking the center of the circle at the right end of the conical shell as the origin O, a column coordinate system (ρ, θ, z) is established. r_0 is the radius of the conical shell end, r_1 is the radius of the other end, and L_1 is the total length of the conical shell. The parameter equation of the conical shell under the column coordinate system can be expressed as

$$\begin{cases} S(\theta, z) = \begin{pmatrix} \rho(z)\cos\theta \\ \rho(z)\sin\theta \\ z \end{pmatrix} \\ \rho(z) = r_0 - \dfrac{r_0 - r_1}{L_1} z \end{cases} \tag{2.6}$$

The cord is wound by the nongeodesic winding method, and the differential equation of the winding trajectory can be expressed as

$$\frac{\mathrm{d}\sin\delta'}{\mathrm{d}z} = -\frac{1}{2E}\frac{\mathrm{d}E}{\mathrm{d}z}\sin\delta' \pm \lambda\sqrt{G}[(k_p - k_m)\sin^2\delta' + k_m] \tag{2.7}$$

where δ' is the winding angle of the cord on the core mold, λ is the slippage coefficient of the cord on the

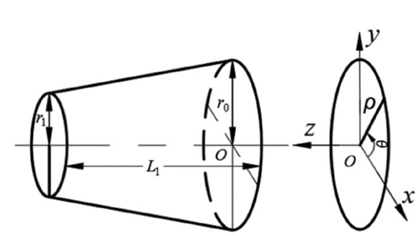

Figure 3: Geometric model of the front-end revolving body.

core mold, the coefficients E and G are the measures of surface $S(\theta, z)$, and k_m and k_p represent the principal curvatures of the surface $S(\theta, z)$. The functional equation can be expressed as

$$E = \left(\frac{\partial S}{\partial \theta}\right)^2 = \rho^2 = \left(r_0 - \frac{r_0 - r_1}{L_1} z\right)^2 \tag{2.8}$$

$$G = \left(\frac{\partial S}{\partial t}\right)^2 = 1 + \left(\frac{\partial \rho}{\partial z}\right)^2 = \frac{(r_0 - r_1)^2}{L_1^2} + 1 \tag{2.9}$$

$$k_m(z) = \frac{d^2\rho(z)}{\mathrm{d}z^2}\left[\left(\frac{\mathrm{d}\rho(z)}{\mathrm{d}z}\right)^2 + 1\right]^{\frac{3}{2}} = 0 \tag{2.10}$$

$$\begin{aligned} k_p(z) &= \frac{-1}{|\rho(z)|\left[\left(\frac{\mathrm{d}\rho(z)}{\mathrm{d}z}\right)^2 + 1\right]^{\frac{1}{2}}} \\ &= -\frac{1}{\left(r_0 - \frac{r_0 - r_1}{L_1} z\right)\left(\frac{(r_0 - r_1)^2}{L_1^2} + 1\right)} \end{aligned} \tag{2.11}$$

2.3.2 Cord trajectory model in the extrusion stage

The capsule extrusion model corresponding to the front-end revolving body of the core mold is shown in Figure 4. MN, NQ, QP, and PM are the four intersecting cord micro-segments in the capsule, R_0 is the curvature radius of the latitudinal surface of the capsule, and points M and Q are on the latitude of the capsule. R_0' is the radius of the corresponding section of the core mold. During the extrusion process, it is assumed that there is no relative sliding between any two intersecting curtain strands. Therefore, the lengths of microsegments MN, NQ, QP, and PM remain constant, and the length of MQ changes.

Since the number of cords wound on the core mold is certain, the radius angle θ_s corresponding to the arc MQ on the certain section of the mandrel remains unchanged after extrusion. According to the geometric structure relationship, the relationship between the cord winding angle before and after the capsule extrusion can be expressed as

$$MN = \frac{R_0\theta_s}{2\sin\delta} = \frac{R_0'\theta_s}{2\sin\delta'}, \tag{2.12}$$

where δ is the cord winding angle after the capsule extrusion. Equation (2.12) can be simplified to

$$\sin\delta' = \sin\delta \cdot \frac{R_0'}{R_0} \tag{2.13}$$

In summary, given the initial winding angle γ and the slippage coefficient λ, equation (2.7) can be solved by the fourth-order Runge-Kutta method to obtain the cord winding angle δ' at each point on the conical shell. After extrusion, equation (2.13) can be solved to obtain the cord winding angle δ at each position of the cylindrical section of the capsule.

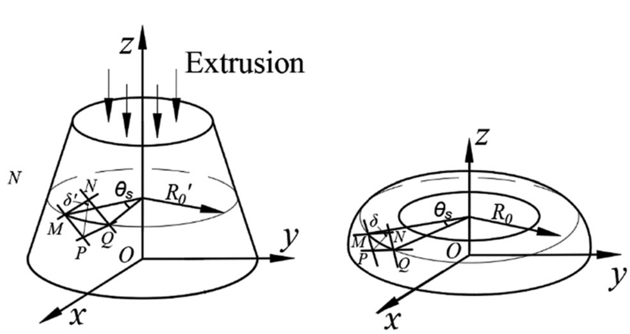

Figure 4: Schematic diagram of the cord winding variation.

3 Solution of the mechanical model

3.1 Solution of capsule state vectors

The air spring in the internal pressure-filled state can be simplified to an axisymmetric rotational shell model. The simplified equations of the geometric and equilibrium equations [17] of the air spring can be expressed as

$$\begin{cases} \varepsilon_\varphi = \dfrac{1}{R_\varphi}\left(\dfrac{\mathrm{d}u}{\mathrm{d}\varphi} + w\right), \\ \varepsilon_\theta = \dfrac{1}{R_\theta}(u\cot\varphi + w), \\ \chi_\varphi = \dfrac{1}{R_\theta}\dfrac{\mathrm{d}\theta_\varphi}{\mathrm{d}\varphi}, \\ \chi_\varphi = \dfrac{1}{R_\theta}\theta_\varphi\cot\varphi, \\ \theta_\varphi = \dfrac{1}{R_\varphi}\left(u - \dfrac{\mathrm{d}w}{\mathrm{d}\varphi}\right). \end{cases} \tag{3.1}$$

$$\begin{cases} \dfrac{\mathrm{d}(R_0 N_\varphi)}{\mathrm{d}\varphi} - R_\varphi\cos\varphi N_\theta + R_0 Q_\varphi = 0 \\ \dfrac{\mathrm{d}(R_0 M_\varphi)}{\mathrm{d}\varphi} - R_\varphi\cos\varphi M_\theta - R_0 R_\varphi Q_\varphi = 0 \\ \dfrac{\mathrm{d}(R_0 Q_\varphi)}{\mathrm{d}\varphi} - R_\varphi R_0\left(\dfrac{N_\varphi}{R_\varphi} + \dfrac{N_\theta}{R_\theta}\right) + R_0 R_\varphi P = 0. \end{cases} \tag{3.2}$$

In equation (3.1), u, v, and w are the displacement components of the rotational shell, and θ_φ and θ_θ are the curvature components. In equation (3.2), Q_φ and Q_θ are the shear components.

The capsule state vector (the state vector consists of six physical quantities: displacement and internal forces) can be denoted as

$$Z = \{u \quad w \quad \theta \quad N_\varphi \quad Q_\varphi \quad M_\varphi\}^T \tag{3.3}$$

By combining equations (2.2), (2.3), (3.1), and (3.2) and using Maple mathematical software to eliminate and transform the variables, the first-order state vector differential equation of the air spring capsule can be expressed as

$$\frac{\mathrm{d}\{Z\}}{\mathrm{d}\lambda} = B\{Z\} + \{q\}, \tag{3.4}$$

where $\{q\} = \{0 \quad 0 \quad 0 \quad 0 \quad -\mathrm{R}_\varphi \mathrm{P} \quad 0\}$. B is the coefficient matrix and can be expressed as

$$B = \begin{bmatrix} B_{11} & B_{12} & 0 & B_{14} & 0 & 0 \\ B_{21} & 0 & B_{23} & 0 & 0 & 0 \\ 0 & 0 & B_{33} & 0 & 0 & B_{36} \\ B_{41} & B_{42} & 0 & B_{44} & B_{45} & 0 \\ B_{51} & B_{52} & 0 & B_{54} & B_{55} & 0 \\ 0 & 0 & B_{63} & 0 & B_{65} & B_{66} \end{bmatrix} \tag{3.5}$$

B_{ij} are the nonzero elements of the matrix B and can be expressed as follows:

$$\begin{aligned}
B_{11} &= -\frac{R_\varphi A_{12}\cos\varphi}{A_{11}R_0}, \quad B_{12} = -\frac{R_\varphi A_{12}\sin\varphi}{A_{11}R_0}, \\
B_{14} &= -\frac{R_\varphi}{A_{11}}, \quad B_{21} = 1, \quad B_{23} = -R_\varphi, \quad B_{33} = -\frac{R_\varphi D_{12}\cos\varphi}{R_0 D_{11}} \\
B_{36} &= \frac{R_\varphi}{D_{11}}, \quad B_{41} = -\frac{R_\varphi \cos^2\varphi A_{12}^2}{R_0^2 A_{11}} + \frac{R\varphi \cos^2\varphi A_{22}}{R_0^2}, \\
B_{42} &= -\frac{R_\varphi \cos\varphi A_{12}^2 \sin\varphi}{R_0^2(\varphi)A_{11}} + \frac{R_\varphi \cos\varphi A_{22}\sin\varphi}{R_0^2}, \\
B_{44} &= -\left(\frac{\mathrm{d}R_0}{\mathrm{d}\varphi}\right)\frac{1}{R_0} + \frac{R_\varphi \cos\varphi\, A_{12}}{R_0 A_{11}}, \quad B_{45} = -1, \\
B_{51} &= -\frac{R_\varphi \cos\varphi A_{12}^2}{R_0 R_\theta A_{11}} + \frac{R_\varphi \cos\varphi A_{22}}{R_0 R_\theta}, \\
B_{52} &= -\frac{R_\varphi \sin\varphi A_{12}^2}{R_0 R_\theta A_{11}} + \frac{R_\varphi \sin\varphi A_{22}}{R_0 R_\theta}, \quad B_{54} = 1 + \frac{R_\varphi A_{22}}{R_0 A_{11}}, \\
B_{55} &= -\left(\frac{\mathrm{d}R_0}{\mathrm{d}\varphi}\right)\frac{1}{R_0}, \\
B_{63} &= \frac{D_{22}\cos^2\varphi R_\varphi}{R_0^2} - \frac{D_{12}^2\cos^2\varphi R_\varphi}{R_0^2 D_{11}}, \quad B_{65} = R_\varphi, \\
B_{66} &= \frac{D_{12}\cos\varphi R_\varphi}{R_0 D_{11}} - \left(\frac{\mathrm{d}R_0}{\mathrm{d}\theta}\right)\frac{1}{R_0}.
\end{aligned}$$

The elements in the state vector equation coefficient matrix A are functions of the coordinate φ. Therefore, equation (3.5) as a variable coefficient nonhomogeneous matrix differential equation is difficult to solve. The state vector equation is first homogenized and made constant, and then solved by the precise integration method.

Equation (3.4) is collapsed to obtain a differential equation with homogeneous expansion and can be expressed as

$$\frac{\mathrm{d}}{\mathrm{d}s}\begin{Bmatrix} Z \\ I \end{Bmatrix} = \begin{bmatrix} B & q \\ 0 & 0 \end{bmatrix}\begin{Bmatrix} Z \\ I \end{Bmatrix}. \tag{3.6}$$

Equation (3.6) can be rewritten as

$$\frac{\mathrm{d}}{\mathrm{d}s}\{\bar{Z}\} = [\bar{B}]\{\bar{Z}\}. \tag{3.7}$$

In equation (3.7), $\{\bar{Z}\}$ is the expansion state vector. Under the condition that the radius change is small enough, the variables in the coefficient matrix A that vary with coordinates φ can be replaced by the corresponding average values. Therefore, A can be considered as a constant matrix, and equation (3.7) can be solved by the precise integration method with high precision.

According to the matrix theory, the ordinary solution for equation (3.7) can be expressed as

$$\{\bar{Z}\}_{\varphi_2} = \exp([\bar{B}](\varphi_2 - \varphi_1))\{\bar{Z}\}_{\varphi_1} = [T_s]\{\bar{Z}\}_{\varphi_2} \tag{3.8}$$

In equation (3.8), T_s is the transfer matrix of the rotational shell in the meridional direction, giving the relationship between the expansion state vectors at two adjacent points φ_1 and φ_2 along the meridian direction. The transfer matrix can be obtained by the precise integration method [18]. After the transfer matrix has been determined, the expansion state vector at the initial point of the capsule can be obtained by the boundary conditions at the starting and end of the rotating shell meridian. Then, the expansion state vector at any point along the meridian of the air spring capsule can be solved by the transfer matrix.

3.2 Solution of mechanical properties

The starting end of the air spring capsule ($\varphi = \alpha$) is radially constrained by the constraint sleeve and is free to move in the axial direction. The boundary conditions can be expressed as

$$\begin{cases} u\cos(\varphi) + w\sin(\varphi)|_{\varphi=\alpha} = 0 \\ u\sin(\varphi) + w\cos(\varphi)|_{\varphi=\alpha} = x \\ M|_{\varphi=\alpha} = 0. \end{cases} \tag{3.9}$$

In equation (3.9), x is the axial displacement value of the air spring.

The end of the air spring capsule ($\varphi = 2\pi - \beta$) is completely fixed to the base. The boundary conditions can be expressed as

$$\begin{cases} u|_{\varphi=2\pi-\beta} = 0 \\ w|_{\varphi=2\pi-\beta} = 0 \\ M|_{\varphi=2\pi-\beta} = 0. \end{cases} \tag{3.10}$$

The stiffness of the air spring can be obtained by the change in the bearing capacity of the air spring under the unit displacement. Under the conditions of axial deformation of the air spring, the expansion state vector at the initial point of the air spring can be solved by changing the displacement values x in the boundary conditions of the air spring. The result is given as

$$\{\bar{Z}\}_{\varphi=\alpha} = \{u_0 \quad w_0 \quad \theta_0 \quad N_0 \quad Q_0 \quad M_0 \quad 1\}. \tag{3.11}$$

By analyzing the force at the starting point of the circular section of the capsule, the bearing capacity of the air spring can be expressed as

$$F = P\pi r_0^2 - ((N_0 \sin(\alpha) - Q_0 \cos(\beta)2\pi r_0) \tag{3.12}$$

From equation (3.12), the bearing capacity of the air spring is determined by the initial capsule state vector and the internal pressure. Due to the complex coupling relationship between the initial state vector of the capsule and the internal pressure, the stiffness characteristics of the air spring are difficult to be solved; it is solved in this article using the iterative integral method. The deformation process of the air spring is decomposed into the superposition of small deformations. In the ith small deformation stage, the following assumptions are made:

(1) Constant structural parameters R_e and R_φ during small deformation.
(2) The small deformation process can be divided into the capsule state change phase and the internal pressure change phase. The axial displacement of the air spring changes and the internal pressure remains unchanged in the capsule state change phase, and the axial displacement of the air spring remains unchanged and the internal air pressure changes in the internal pressure change phase.

During the capsule state vector change phase, the air spring displacement value changes from x_{i-1} to x_i, and the internal pressure remains as P_{i-1}. By changing the value of x in equation (3.9), the initial state vector of the capsule under different boundary conditions is solved, and the bearing variation force ΔF_{i1} under the condition of the internal pressure P_{i-1} is calculated. During the internal air pressure change phase, the air spring displacement remains constant at x_i, and the internal air pressure changes from P_{i-1} to P_i. The bearing variation force ΔF_{i2} of the air spring is calculated by changing the air pressure under the same boundary conditions as displacement x_i.

According to the adiabatic equation [20], the relationship between the internal pressure and internal volume of air spring can be expressed as

$$(P_a + P_{i-1})V_{i-1}{}^n = (P_a + P_i)V_i^n \tag{3.13}$$

where P_a is the atmospheric pressure, P_{i-1} and V_{i-1} are the internal pressure and volume values of the air spring at the axial displacement x_{i-1}, respectively, P_i and V_i are the internal pressure and volume values of the air spring at the axial displacement x_i, respectively, and n is the polytropic coefficient.

(3) After each small deformation, the air spring capsule is still regarded as an arc, and the relationship between the structural parameters R_e and R_φ of the air spring and the axial displacement x can be expressed as [19]

$$\begin{cases} R_e^i = R_e^{i-1} + A_R(x_i - x_{i-1}) \\ R_\varphi^i = R_\varphi^{i-1} + A_{R_\varphi}(x_i - x_{i-1}) \\ A_{R_e} = \dfrac{(2\pi - \alpha - \beta)\cos\alpha\cos\beta + \sin(\alpha+\beta)}{2[1-\cos(\alpha+\beta)] + (2\pi-\alpha-\beta)\sin(\alpha+\beta)} \\ A_{R_\varphi} = -\dfrac{(\cos\beta - \cos\alpha)}{(2(1-\cos(\beta+\alpha)) + (2\pi-\beta-\alpha)(\sin(\beta+\alpha))} \end{cases} \tag{3.14}$$

Based on the above assumption, the stiffness of the air spring can be expressed as

$$K = \sum_{i=1}^{m}(\Delta F_{i1} + \Delta F_{i2})/x_m \tag{3.15}$$

For the rubber-cord composite, the Tsai–Hill strength theory can be used for failure determination. The Tsai–Hill's failure criterion can be expressed as

$$\frac{\sigma_1^2}{X^2} - \frac{\sigma_1\sigma_2}{X^2} + \frac{\sigma_2^2}{Y^2} + \frac{\tau_{12}^2}{S^2} = 1 \tag{3.16}$$

where X is the axial tensile strength of the composite, Y is the transverse tensile strength of the composite, and S is the shear strength of the composite.

According to the material model of the air spring, the relationship between the stress components σ_1, σ_2, and τ_{12} in the main direction of the rubber-cord composite and the strain components ε_φ and ε_θ in the main direction of the capsule can be expressed as

$$\begin{Bmatrix} \sigma_1 \\ \sigma_2 \\ \sigma_{12} \end{Bmatrix} = [T][\bar{Q}]\begin{bmatrix} \varepsilon_\varphi \\ \varepsilon_\theta \\ 0 \end{bmatrix} \tag{3.17}$$

The strain components ε_φ and ε_θ can be solved by equation (3.1). T is the rotation axis matrix, and the parameter equation can be expressed as

$$T = \begin{bmatrix} \cos^2\delta & \sin^2\delta & 2\sin\delta\cos\delta \\ \sin^2\delta & \cos 2\delta & -2\sin\delta\cos\delta \\ -\sin\delta\cos\delta & \sin\delta\cos\delta & \cos^2\delta - \sin^2\delta \end{bmatrix} \quad (3.18)$$

4 Computational analysis and experimental verification

The stiffness characteristics and burst pressure of a certain type of the cord-reinforced air spring with winding formation are calculated and analyzed, and the structural parameters of the air spring are shown in Table 1.

4.1 Computational analysis

4.1.1 Effects of material parameters

The material properties of the rubber-cord composite are the elastic constants and the fundamental strengths. The elastic constants mainly affect the stiffness characteristic of the air spring, and the fundamental strengths mainly affect the burst pressure of the air spring. Since the elastic modulus E_2 is much smaller than the elastic modulus E_1 and the shear modulus G_{12}, only the elastic modulus E_1 and the shear modulus G_{12} are scaled by a certain number to investigate the influence of the elastic constants in the analysis process. The calculated results are shown in Figure 5, and the elastic modulus E_1 has a greater influence on stiffness characteristics.

The burst pressure of the air spring is calculated by scaling the fundamental strengths X, Y, and Z of the material by the same value. The calculated results are shown in Figure 6. As the fundamental strengths increases, the burst pressure of the air spring increases significantly. However, the axial tensile strength and shear strength have basically no effect on the burst pressure of the air spring. Therefore, the rubber-cord composite with higher transverse tensile strength can be selected to increase the burst pressure of the air spring.

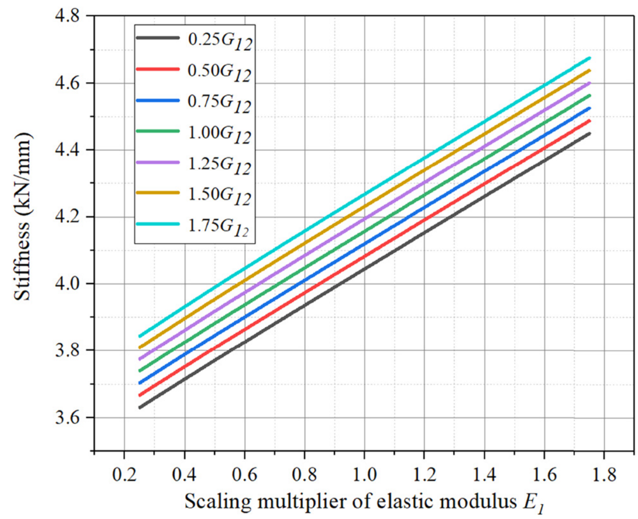

Figure 5: Effect of elastic constants on the stiffness characteristics.

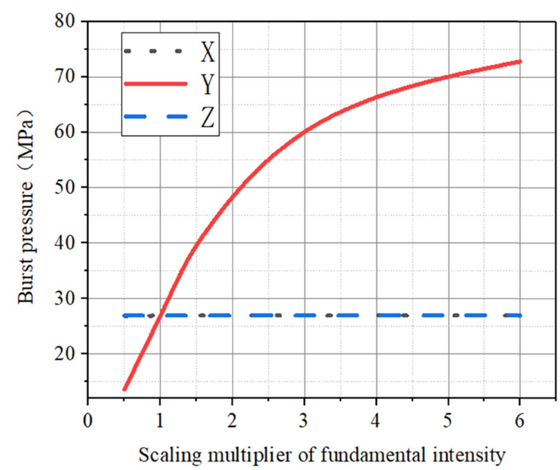

Figure 6: Effect of fundamental strengths on the burst pressure.

Table 1: Structural parameters of the air spring

Name	Value	Name	Value	Name	Value
R_φ	22.5 mm	λ	0.2	X	347.6 Mpa [20]
R_e	141 mm	E_1	49.7 GPa	Y	4.7 MPa [20]
α	90°	E_2	6 MPa	Z	4.0 MPa [20]
β	54°	G_{12}	2.5 MPa	h	3.3 mm
γ	24.8°	ν_{21}	0.45		

4.1.2 Effects of winding parameters

The winding pattern is determined after the initial winding angle and the slippage coefficient of the cord are determined for the certain core mold. According to the actual engineering experience, the slippage coefficient of the cord does not exceed 0.25; otherwise, the cord will slide during the winding process. In addition, for the core mold used for the certain type of air spring in this article, the initial winding angle of the cord does not exceed 34.2° to ensure that the winding angle during cord winding does not exceed 90° under the above conditions. The stiffness

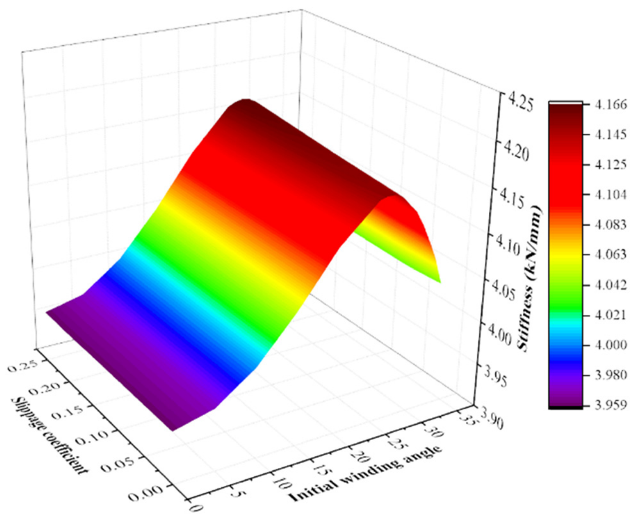

Figure 7: Effect of winding parameters on the stiffness characteristics.

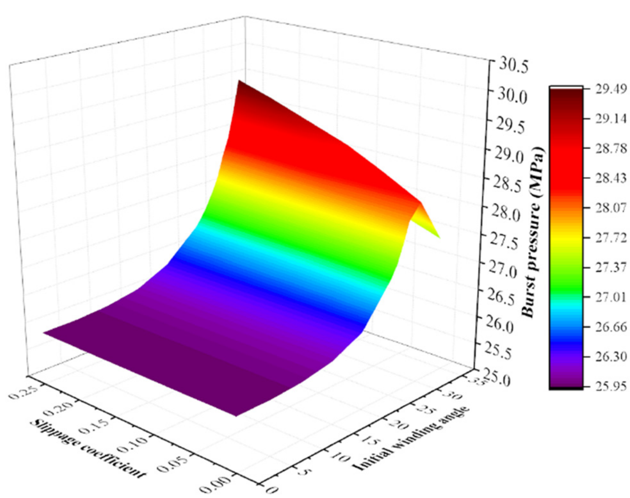

Figure 8: Effect of winding parameters on the burst pressure.

characteristic and burst pressure of the air spring under different initial winding angles and slippage coefficients are calculated. The results are shown in Figures 7 and 8, respectively. The stiffness and burst pressure increase and then decrease with the increase in the initial winding angle. The stiffness reaches the highest near 25.2°, and the burst pressure reaches the highest near 30.6°. The influence of the slippage coefficient on the mechanical properties is low. However, it increases with the increase in the initial winding angle. The cord winding parameters have a large impact on the burst pressure. Therefore, under the condition of ensuring the basic requirements of stiffness characteristics, the cord winding angle and the slippage coefficient can be determined based on the strength requirements in the air spring design process.

4.1.3 Effects of structural parameters

The structural design parameters of the air spring are R_φ, R_e, α, and β. R_e is a definite value for the certain type of air spring with a definite bearing capacity, and therefore, we consider only the effect of the structural parameters R_φ, α, and β on the mechanical properties of the air spring. Under the condition that the structure coefficient is scaled, and the corresponding changes in the stiffness characteristic and burst pressure are calculated as shown in Figure 9. The burst pressure and stiffness of the air spring increase as the structural parameter R_φ increases and the stiffness characteristics are further affected.

The range of α and β is [0–90°]. The stiffness and the burst pressure of the air spring are calculated with different values of α and β. The results are shown in Figures 10 and 11. Compared to parameter α, parameter β has a

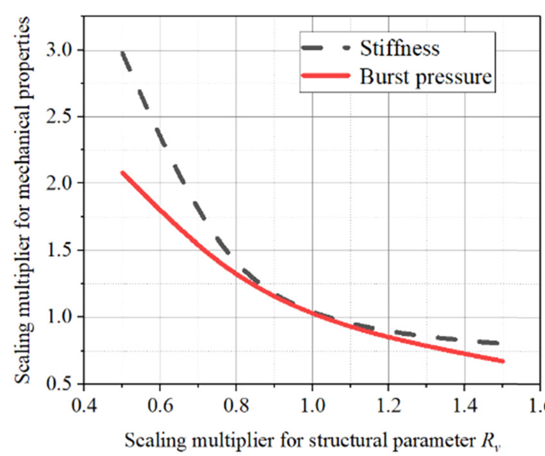

Figure 9: Effect of the ripple radius on the stiffness and burst pressure.

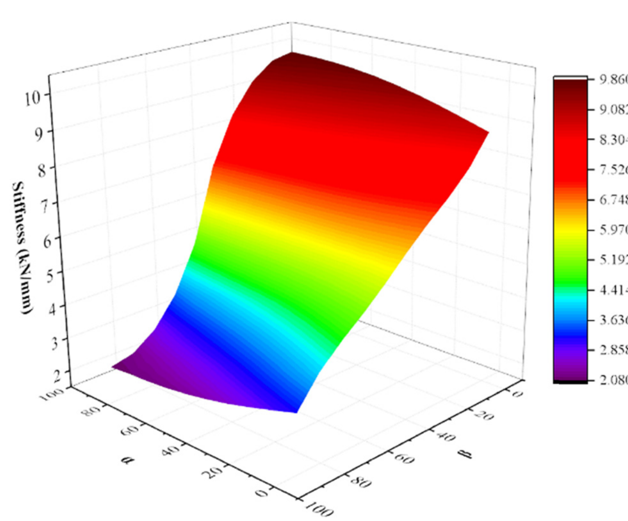

Figure 10: Effect of guide angles on the stiffness characteristics.

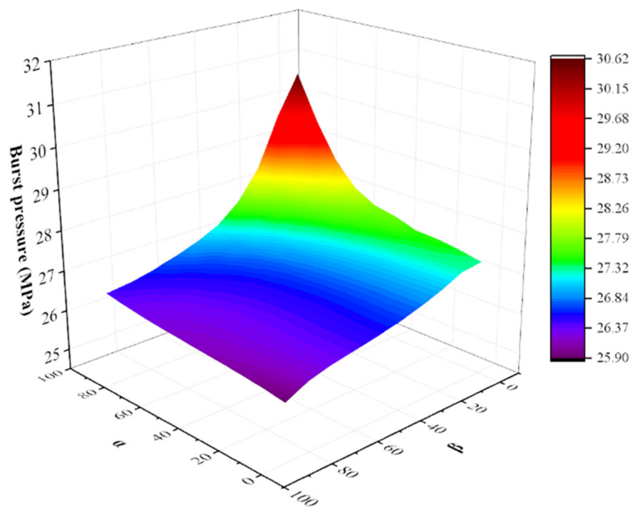

Figure 11: Effect of guide angles on the burst pressure.

Table 2: Mechanical performance test results

Name	Prototype number	Theoretical calculation value	Experimental results	Calculati-on errors (%)
Stiffness	SZ-01	4.16 kN/mm	4.34 kN/mm	4.15
	SZ-02		4.12 kN/mm	0.97
	SZ-03		4.28 kN/mm	2.80
	SZ-04		4.37 kN/mm	4.81
	SZ-05		4.06 kN/mm	2.46
	SZ-06		4.08 kN/mm	1.96
	SZ-07		4.45 kN/mm	6.52
	SZ-08		4.41 kN/mm	5.67
	SZ-09		4.50 kN/mm	7.56
	SZ-10		4.54 kN/mm	8.37
Burst pressure	SZ-11	26.92 MPa	25.4 MPa	5.98
	SZ-12		27.0 MPa	0.30
	SZ-13		25.0 MPa	7.68

greater effect on the stiffness of the air spring. The stiffness of the air spring decreases as the parameter β increases and the stiffness is the smallest with $\alpha = \beta = 90°$. Parameters α and β have little effect on the burst pressure. The burst pressure increases with the growth of parameter α and decreases with the growth of parameter β. The highest burst pressure of the air spring is achieved with $\alpha = 90°$ and $\beta = 0°$.

4.2 Test verification

The mechanical properties of the air spring are tested, and the test installation is shown in Figure 12. A total of 10 air springs were tested for stiffness and three air springs were tested for the burst pressure. The results of the mechanical properties of the air spring in the rated state are shown in Table 2. The theoretical calculation errors are within 10%, and the theoretical calculation results are in good agreement with the test results.

5 Conclusion

In this article, a nonlinear capsule mechanics model with complex winding trajectory variation characteristics is constructed based on the thin-shell theory, the nongeodesic winding model, and the assumption of cord cross-stability. Then, the capsule state vector is solved by the extended homogeneous capacity precision integration method. The stiffness characteristic and burst pressure of the air spring are calculated based on the iterative integration method and Tsai–Hill strength theory, respectively. Finally, the effects of winding parameters, material properties, and geometric structure parameters on the

(a) (b)

Figure 12: Installation diagram of the air spring mechanical characteristics test: (a) stiffness test and (b) burst pressure test.

mechanical properties of the air spring are discussed, and the theoretical model is verified to be highly accurate. Based on the above results, the following conclusions can be summarized.

(1) The stiffness of an air spring increases with the growth of the capsule elastic constant, and the burst pressure increases significantly with the growth of the transverse tensile strength. Therefore, the rubber-cord composite with the low elastic constant and the high transverse tensile strength can be selected to ensure low stiffness and high reliability of the air spring.
(2) The winding parameters have a large influence on the burst pressure of air springs and a small effect on the stiffness characteristics. Therefore, the winding parameters can be adjusted to effectively increase the burst pressure of the air spring under the condition of ensuring the basic requirements of the stiffness characteristics. In addition, generally winding parameters are defined to maximize the stiffness and burst pressure of the air spring.
(3) The structural parameter R_φ of the air spring has a large effect on the stiffness characteristics and burst pressure. The stiffness and burst pressure of the air spring increase as the parameter R_φ increases. The effect of parameters α and β on the burst pressure of the air spring are small. The effect of parameters α and β on the stiffness of the air spring are large, especially the parameter β. The stiffness decreases as the growth of parameter β, and it reaches a minimum value with $\alpha = \beta = 90°$.

Conflict of interest: There are no conflicts of interest.

References

[1] Mazzola L, Berg M. Secondary suspension of railway vehicles-air spring modeling: performance and critical issues. J Rail Rapid Transit. 2014 Mar 13;228(3):225–41.
[2] Liu YB, Li M, He L. Nonlinear dynamics of the marine air-bag vibration isolation system. J Ship Mech. 2015;9(11):1385–92. Chinese.
[3] Lee SJ. Development and analysis of an air spring model. Int J Automot Technol. 2010 Jul 21;11(4):471–9.
[4] Fongue WA. Air spring air damper: modelling and dynamic performance in case of small excitations. Int J Passeng Cars-Mech Syst. 2013 May 13;6(2):1196–208.
[5] Lee JH, Kim KJ. Modeling of nonlinear complex stiffness of dual-chamber pneumatic spring for precision vibration isolations. J Sound Vib. 2007 Apr 3;301(3–5):909–26.
[6] Asami T, Yokota Y, Ise T, Honda I, Sakamoto H. An approximate formula to calculate the restoring and damping forces of an air spring with a small pipe. J Vib Acoust. 2013 Jul 1;135(5):592–8.
[7] Li XB, Li T. Research on vertical stiffness of belted air springs. Veh Syst Dyn. 2013 Jul 26;51(11):1655–73.
[8] Li XB, He Y, Liu WQ, Wei YT. Research on the vertical stiffness of a rolling lobe air spring. Proc Inst Mech Eng Part F J Rail Rapid Transit. 2015 May 19;230(4):1172–83.
[9] Erin C, Wilson B, Zapfe J. An improve model of a pneumatic vibration isolator: theory and experiment. J Sound Vib. 1998 Nov 19;218(1):81–101.
[10] Moon JH, Lee BG. Modeling and sensitivity analysis of a pneumatic vibration isolation system with two air chambers. Mech Mach Theory. 2010 Sep 17;45(12):1828–50.
[11] Wong PK, Xie ZC, Zhao J, Xu T, He F. Analysis of automotive rolling lobe air spring under alternative factors with finite element model. J Mech Sci Technol. 2014 Dec 12;28(12):5069–81.
[12] Rojas EV, Chapelle D, Perreux D, Delobelle F, Thiebaud F. Unified approach of filament winding applied to complex shape mandrels. Compos Struct. 2014 Jun 20;116:805–13.
[13] Fu J, Yun J, Jung Y. Filament winding path generation based on the inverse process of stability analysis for non-axisymmetric mandrels. J Composite Mater. 2016 Dec 12;51(21):2989–3002.
[14] Wang R, Jiao W, Liu W, Yang F, He XD. Slippage coefficient measurement for non-geodesic filament-winding process. Compos A Appl Sci Manuf. 2010 Dec 5;42(3):303–9.
[15] Peters ST. Composite filament winding. America: ASM International; 2011.
[16] Jiao GQ, Jia PR. Mechanical of composite materials. Beijing: Beihang University Press; 2007.
[17] Xu ZL. Elasticity. Beijing: Higher Education Press; 2016.
[18] Zhong WX, Williams FW. A precise time step integration method. J Mech Eng Sci. 1994 Nov 1;208(6):427–30.
[19] He L, Zhao YL. Theory and design of high-pressure and heavy-duty air spring for naval vessels. J Vib Eng. 2013;26(6):886–94. Chinese.
[20] Gao H, Shuai CG, Ma JG, Xu GM. Study on theoretical model of burst pressure of fiber reinforced arc-shaped rubber hose with good balance performance. Polym Polym Compos. 2020 Aug 17;29(5):470–283.